

High Signal-to-Noise Ratio Contrast-Enhanced Photoacoustic Imaging using Acoustic Sub-Aperture Processing and Spatiotemporal Filtering

Ge Zhang¹, Bingxue Wang¹, Antonio Stanziola¹, Anant Shah², Jeffrey Bamber², and Meng-Xing Tang¹

¹ Department of Bioengineering, Imperial College London, London, United Kingdom

² Joint Department of Physics and CRUK Cancer Imaging Centre, The Institute of Cancer Research and The Royal Marsden NHS Foundation Trust, London, United Kingdom

Email: Mengxing.Tang@Imperial.ac.uk

Abstract— Contrast-enhanced photoacoustic imaging has shown great potential in medical imaging applications. Despite the obvious advantages of contrast enhancement, contrast agent signals attenuate significantly during the propagation process and can be masked by noise and clutter signals generated by tissue, resulting in the reduction of imaging sensitivity. In this study, we demonstrate that acoustic sub-aperture processing (ASAP) may be adapted to process photoacoustic images to generate high signal-to-noise ratio (SNR) images compared to the conventional spatiotemporal filtered images. Experiments were performed *in vitro* on a 0.6-mm diameter tube in a tissue-mimicking phantom containing a previously demonstrated exogenous photoacoustic contrast agent, Cyanine 7.5-coated nanodroplets. Data were acquired using a preclinical multispectral optoacoustic tomography (MOST) system. The results suggested that ASAP-assisted spatiotemporal filtering can improve SNR by about 8 dB *in vitro* compared to that without using ASAP. Besides flow imaging, this technique can also potentially benefit other photoacoustic imaging applications such as molecular imaging and super-resolution imaging.

Keywords— Droplets, Acoustic Sub-aperture Processing, Optical Vaporization, Multispectral Optoacoustic Tomography (MSOT)

I. INTRODUCTION

Photoacoustic imaging is an emerging biomedical imaging modality that enables the visualization of biological structures with high-resolution and multi-contrast images [1]. Light absorption by endogenous chromophores or exogenous photoacoustic contrast agents induces transient thermoelastic expansion, causing acoustic waves to be launched and detected by ultrasound transducer to form images through reconstruction algorithms such as back-projection and phased array beamforming principles [2].

Therefore, the contrast of photoacoustic images arises from the optical absorbing properties of the targets against the background. Many studies have been carried out to find novel exogenous photoacoustic contrast agents to provide extra sources of contrast. For example, gold nanoparticles are very popular for their high photophysical flexibility and the capability of increasing the probability of target-binding [3].

Polymer nanoparticles and encapsulations are also very promising as they can help deliver other targeting signalling compounds by incorporating with them, enabling multimodal photoacoustic imaging [4]. Flowing absorbers like magnetic polyethylene microspheres are preferred as they can provide continuous contrast agent signals [5], [6]. Besides, dual-contrast agents that can generate both optical and ultrasound contrast enhancement like indocyanine green (ICG)-loaded perfluorocarbon (PFC) nanodroplets, PFC nanodroplets encapsulated with gold nanorods and silica-coated lead sulfide (PbS) nanoparticles, and Cyanine 7.5-dyed, lipid-coated nanodroplets were also widely investigated in photoacoustic molecular imaging applications [7]–[10].

However, photoacoustic imaging suffers from signal-to-noise (SNR) issues when imaging beyond a few centimeters in depth. The strong optical scattering property of most biological tissues makes the penetration depth of photoacoustic signals limited. To address this problem, a spatiotemporal clutter filter demonstrated by Deffieux *et al.* [11] can be used to remove the tissue motion artefacts using singular value decomposition (SVD) processing and improves the sensitivity of ultrasound imaging. Nonetheless, apart from the clutter signals, random noise and interference signals also reduce the imaging contrast. Acoustic Sub-Aperture Processing (ASAP) has been shown to be able to remarkably improve the signal-to-noise ratio (SNR) of contrast-enhanced ultrasound imaging by removing random noise using cross-correlation and suppressing interference signals [12].

The aim of this study was to integrate ASAP with the spatiotemporal filtering technique using SVD to distinguish vascular signals from background signals and increase the SNR of the contrast-enhanced photoacoustic images of an *in vitro* tissue-mimicking phantom examined in a multispectral optoacoustic tomography (MOST) system.

II. METHODS AND EXPERIMENT

A. Nanodroplet Preparation

The lipid-encapsulated, decafluorobutane (DFB)-filled Cy-microbubbles precursor were manufactured using a

formulation described by Sheeran *et al.* [13]. The lipid mixture was composed of 1,2-dipalmitoyl-sn-glycero-3-phosphocholine (DPPC), 1,2-dipalmitoyl-sn-glycero-3-phosphoethanolamine-N-[methoxy (polyethylene glycol)-2000] (16:0 PEG2000 PE) and DSPE-PEG (2000)-Cyanine7.5 dissolved in a solution of propylene glycol, glycerol, and phosphate-buffered saline (PBS). Then this lipid solution was sealed in a glass vial and the headspace vial was purged with DFB gas at room temperature. Cy-microbubble precursors were then generated via mechanical agitation and the Cy-droplet solution was finally obtained by the condensation of Cy-microbubbles using the method detailed in Li *et al.* [14].

B. In vitro tissue mimicking phantom setup

A tissue-mimicking agar phantom was prepared for the *in vitro* experiment. A semi-transparent silicone tube (inner diameter=0.6 mm, outer diameter=1.2mm, Harvard Apparatus, UK) was embedded in the center of the cylindrical phantom (diameter=40mm). The agar-intralipid gel was manufactured according to the method described by Madsen *et al.* [15], 2% w/v agar powder (Fisher Scientific, UK) and 1% v/v intralipid (20% emulsion, Sigma, UK) in deionized and distilled water was used to produce the agar solution. Then the 10% diluted Cy-droplet solution was used for imaging.

C. Imaging acquisition and beamforming

The photoacoustic imaging process was performed at a single wavelength of 788 nm, which is the peak absorption of Cyanine 7.5 with a fluence estimated to be 20 mJ/cm² per pulse for each image. The raw radiofrequency (RF) data was acquired over 10s at a 10 Hz pulse repetition frequency using the multispectral optoacoustic tomography (MSOT) system (inVision 256TF, iThera Medical) with a 256-element transducer covering a field of view of 270°, which is referred as MSOT 256. Photoacoustic images were then reconstructed by extracting and beamforming these RF data using a customized back-projection algorithm in Matlab. A temporal delay for each channel was applied according to their different positions along the 270° concave transducer array. The geometry parameters were applied according to the MSOT transducer design described by Dima *et al.* [16]. Afterwards, information from each channel was summed over all the 256 channels to form the final image for each frame and an image sequence with 100 frames was acquired.

D. ASAP-assisted SVD processing

As illustrated in Fig 1, for ASAP-assisted SVD processing method, RF data collected from 256 channels was equally split into two groups in an alternating pattern. Then each set of data extracted from 128 channels was beamformed

individually to reconstruct an image for one sub-aperture and two image data sets were obtained. Singular value decomposition processing was applied to each image data set subsequently to remove the clutter signals by rejecting the first several singular vectors that are related to tissue. Next, these two sets of SVD-filtered images were cross-correlated over the 100 frames to generate the final ASAP SVD-filtered image. This image was then compared with the image after SVD filtering and averaging over the same data set but without ASAP.

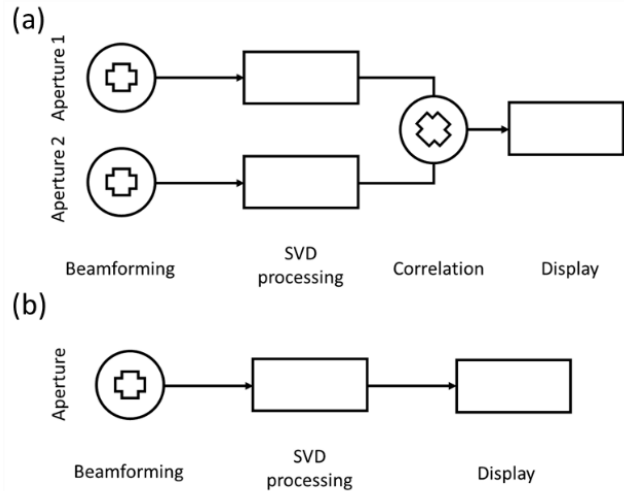


Fig 1. (a) Schematic of the ASAP-assisted SVD processing method. For each frame, RF data from all the 256 channels was split into two sub-apertures and beamformed separately. These two sets of data were then filtered individually and correlated temporally. (b) Schematic of conventional beamforming and filtering method. The RF data from all the 256 channels was directly beamformed and filtered without any splitting of channels and the process of cross-correlation.

III. RESULTS AND DISCUSSIONS

Fig 2 shows the comparison between the summations of beamformed, SVD-filtered and ASAP-assisted SVD filtered images, respectively, for the same acquisition data set. In Fig 2 (a), the tube inside the agar phantom cannot be seen due to the low SNR. After SVD processing, a tube can be identified in Fig 2 (b). Furthermore, the noise floor in Fig 2 (c) was significantly reduced after ASAP SVD filtering compared to that of Fig 1 (b). The power intensity of the signal (within the tube) and noises (outside the phantom) indicated by the green dashed circles were measured and results show that SNR was improved by approximately 8 dB in ASAP SVD-filtered images compared to SVD-filtered image while maintaining the resolution level.

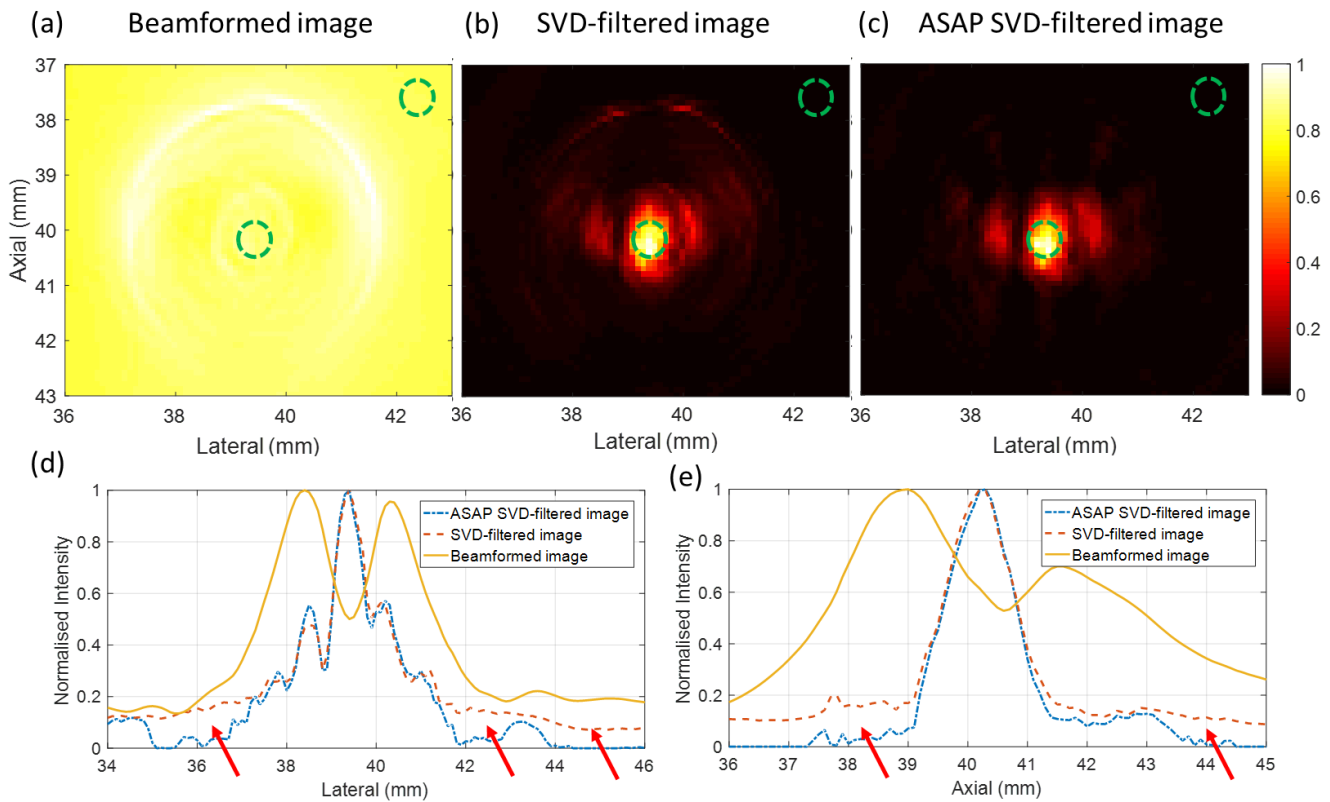


Fig 2. (a) *In vitro* results, showing the cross-section of a 0.6 mm-diameter tube in a 4 mm diameter agarose phantom with flowing Cy-7.5 nanodroplets by summation of 100 (a) beamformed images, (b) SVD-filtered images, and (c) ASAP SVD-filtered images, respectively, for the same acquisition. (d) and (e) show the profiles in lateral and axial directions of these images.

IV. CONCLUSION

In this study, we demonstrate that ASAP could be adapted to improve the signal-to-noise ratio of photoacoustic images of flow. The results suggested that ASAP-assisted filtering can generate a SNR improvement of around 8 dB *in vitro* compared to the conventional filtering technique without ASAP. Its effect *in vivo* needs further research. The improved image quality by ASAP-assisted spatiotemporal processing may benefit general photoacoustic imaging applications including molecularly-targeted imaging and super-resolution imaging.

ACKNOWLEDGMENT

The authors would like to thank all the ultrasound lab for imaging and sensing (ULIS) group members for their valuable advice. The authors would like to also thank the funding bodies: Engineering and Physical Sciences Research Council (EPSRC): EP/N015487/1, EP/N014855/1, EP/M011933/1, Strategic Equipment Grant EP/N015266/1, Cancer Research UK (CRUK): Multidisciplinary Project Award (C53470/A22353), the Institute of Cancer Research CRUK Cancer Imaging Centre (C1060/A16464).

REFERENCES

- [1] P. Beard, "Biomedical photoacoustic imaging," *Interface Focus*, vol. 1, no. 4, pp. 602–631, 2011.
- [2] L. Wang and S. Hu, "NIH Public Access," *Science (80-.)*, vol. 335, no. 6075, pp. 1458–1462, 2012.
- [3] J. K. Fard, S. Jafari, and M. A. Eghbal, "A review of molecular mechanisms involved in toxicity of nanoparticles," *Adv. Pharm. Bull.*, vol. 5, no. 4, pp. 447–454, 2015.
- [4] J. Weber, P. C. Beard, and S. E. Bohndiek, "Contrast agents for molecular photoacoustic imaging," *Nat. Methods*, vol. 13, no. 8, pp. 639–650, 2016.
- [5] X. L. Dean-Ben and D. Razansky, "Localization optoacoustic tomography," *Nat. Publ. Gr.*, vol. 7, no. 4, pp. 18004–18005, 2017.
- [6] S. Vilov, B. Arnal, and E. Bossy, "Overcoming the acoustic diffraction limit in photoacoustic imaging by localization of flowing absorbers," vol. 42, no. 21, pp. 4379–4382, 2017.
- [7] A. Hannah, G. Luke, K. Wilson, K. Homan, and S. Emelianov, "Indocyanine green-loaded photoacoustic nanodroplets: Dual contrast nanoconstructs for enhanced photoacoustic and ultrasound imaging," *ACS Nano*, vol. 8, no. 1, pp. 250–259, 2014.
- [8] K. Wilson, K. Homan, and S. Emelianov, "Biomedical photoacoustics beyond thermal expansion using triggered nanodroplet vaporization for contrast-enhanced imaging," *Nat. Commun.*, vol. 3, pp. 610–618, 2012.
- [9] I. Gorelikov, M. Rui, M. Kolios, E. Strohm, and N. Matsuura, "Vaporization of perfluorocarbon droplets using optical irradiation," *Biomed. Opt. Express*, vol. 2, no. 6, p. 1432, 2011.
- [10] S. Lin *et al.*, "Optically and acoustically triggerable sub-micron phase-change contrast agents for enhanced photoacoustic and ultrasound imaging," *Photoacoustics*, vol. 6, pp. 26–36, 2017.
- [11] T. Deffieux *et al.*, "Spatiotemporal Clutter Filtering of Ultrafast Ultrasound Data Highly Increases Doppler and fUltrasound Sensitivity," *IEEE Trans. Med. Imaging*, vol. 34, no. 11, pp. 2271–2285, 2015.

- [12] C. H. Leow, M.-X. Tang, P. D. Weinberg, A. Stanzola, and E. Bazigou, "ASAP: Super-Contrast Vasculature Imaging Using Coherence Analysis and High Frame-Rate Contrast Enhanced Ultrasound," *IEEE Trans. Med. Imaging*, vol. 37, no. 8, pp. 1847–1856, 2018.
- [13] P. S. Sheeran, S. Luois, P. A. Dayton, and T. O. Matsunaga, "Formulation and acoustic studies of a new phase-shift agent for diagnostic and therapeutic ultrasound," *Langmuir*, vol. 27, no. 17, pp. 10412–10420, 2011.
- [14] S. Li, S. Lin, Y. Cheng, T. O. Matsunaga, R. J. Eckersley, and M. X. Tang, "Quantifying Activation of Perfluorocarbon-Based Phase-Change Contrast Agents Using Simultaneous Acoustic and Optical Observation," *Ultrasound Med. Biol.*, vol. 41, no. 5, pp. 1422–1431, 2015.
- [15] E. L. Madsen, G. R. Frank, and F. Dong, "Liquid or solid ultrasonically tissue-mimicking materials with very low scatter," *Ultrasound Med. Biol.*, vol. 24, no. 4, pp. 535–542, 1998.
- [16] A. Dima, N. C. Burton, and V. Ntziachristos, "Multispectral optoacoustic tomography at 64, 128, and 256 channels," *J. Biomed. Opt.*, vol. 19, no. 3, p. 036021, 2014.